Applied Catalysis B: Environmental 104 (2011) 151–160

Contents lists available at ScienceDirect

Applied Catalysis B: Environmental

journal homepage: www.elsevier.com/locate/apcatb

Effects of temperature and reductant type on the process of NO_x storage reduction over $Pt/Ba/CeO_2$ catalysts

Xiaoying Wang, Yunbo Yu, Hong He*

State Key Laboratory of Environmental Chemistry and Ecotoxicology, Research Center for Eco-Environmental Sciences, Chinese Academy of Sciences, Beijing 100085, PR China

ARTICLE INFO

Article history:
Received 10 July 2010
Received in revised form 6 January 2011
Accepted 16 February 2011
Available online 23 February 2011

Keywords:
NO_x storage reduction
NO_x removal efficiency
Temperature
Reductants
H_2
CO
C_3H_6
$Pt/Ba/CeO_2$

ABSTRACT

The influences of temperature and reductant type on NO_x storage and reduction behavior were studied by transient lean/rich cycles and *in situ* diffuse reflectance infrared Fourier transform spectroscopy (DRIFTS) experiments over $Pt/Ba/CeO_2$ catalysts. It is found that the reducing ability of H_2 is more predominant than that of CO and C_3H_6 especially at low temperatures. DRIFTS results showed that NO_x can be stored as nitrates on both Ba and Ce sites by replacing carbonates species during the lean phase. During the rich phase, however, H_2 regenerated Ba storage sites more effectively than did CO and C_3H_6, and $Ba(NO_3)_2$ could be easier reduced than $Ce(NO_3)_4$. The relatively low reduction performance of CO was attributed to Pt sites being poisoned by CO, which affected low temperature performance, and by carbonates formation, which affected high temperature conversions. The least reactivity of C_3H_6 was due to its lowest activation ability by the catalysts. Furthermore, water addition had a positive effect on CO reduction ability at 200 °C but little influence at elevated temperatures. It was assumed that H_2O improved the low temperature NO_x reduction process by alleviating CO poisoning of Pt.

1. Introduction

Due to its fuel efficiency, the lean burn engine is considered one of the most promising technologies to meet the world's energy crisis. Furthermore, its reduced CO_2 emissions make it attractive for climate change mitigation. Lean-burn exhaust, however, usually contains large amounts of NO_x. As more stringent vehicle emission standards for NO_x are implemented to protect the environment, exhaust purification has become an urgent problem for lean-burn engines [1].

For decades, people have been committed to the development of new technologies to eliminate NO_x emission from lean-burn exhaust. One of the most promising solutions is the use of NO_x storage reduction (NSR, also noted as lean NO_x trap, LNT) catalysts [2]. The NSR catalyst, which was first developed by the Toyota Company, usually contains noble metals (Pt, Pd, Rh), alkali or alkaline earth metals (e.g., Ba), and a high surface area support. This catalyst is supposed to reduce NO_x emission under a cyclic lean/rich mode for diesel or lean-burn gasoline engines. In a typical lean engine operation, NO is oxidized to NO_2 over noble metals and then stored as nitrites and/or nitrates on the storage components of the catalysts. After switching periodically to fuel-rich conditions, the absorbed NO_x is released and reduced to N_2 by hydrogen (H_2), carbon monoxide (CO), and hydrocarbons (HC) [3–6].

Commonly, Al_2O_3 is applied as the support of NSR catalysts due to its high surface area. Recent studies have, however, reported on the advantages of CeO_2 as an important component for three-way catalysts, particularly in relation to its good oxygen storage capacity, and its ability to maintain a high dispersion of noble metals and improve the water-gas shift reaction [7–10]. Keeping these in mind, CeO_2 has been used as either an additive or support in NSR catalysts, and its role varies according to research focus [11–18]. When CeO_2 was used as the support of NSR catalysts, more attempts towards NO_x storage capacity, regeneration ability, thermal stability, and sulfur resistance have been made. It has been reported that the NO_x storage capacity of $Pt/Ba/CeO_2$ is related to the loading of Ba and the thermal stability of surface $BaCO_3$ [14,19]. When Ba loading was lower than 10 wt%, $Pt/Ba/CeO_2$ possesses a higher NO_x storage capacity than ZrO_2, Al_2O_3, and SiO_2 supported catalysts. When Ba loading was up to 16.7 wt%, the NO_x storage capacity of $Pt/Ba/CeO_2$ decreased compared with ZrO_2 and Al_2O_3 supported catalysts. The authors proposed that $BaCO_3$, which can be decomposed at low temperatures (LT-$BaCO_3$), was the most efficient Ba-phase for NO_x storage, and LT-$BaCO_3$ were abundant at lower Ba loadings on ceria supported catalysts. However, CeO_2 supported catalysts with C_3H_6 as the reductant exhibited inferior regeneration activity compared to Al_2O_3 supported catalysts due to a faster reoxidation of

* Corresponding author at: PO Box 2871, 18 Shuangqing Road, Haidian District, Beijing 100085, PR China. Tel.: +86 10 62849123; fax: +86 10 62849123.
E-mail address: honghe@rcees.ac.cn (H. He).

0926-3373/$ – see front matter © 2011 Elsevier B.V. All rights reserved.
doi:10.1016/j.apcatb.2011.02.018

Pt particles during the lean phase [20]. To avoid such influence, a pre-reduction treatment at mild conditions was suggested to reactivate Pt on Pt/Ba/CeO_2, leading to significant enhancement in NSR performance. The thermal stability of Pt/Ba/CeO_2 was also compared with conventional Pt/Ba/Al_2O_3 [21,22]. After thermally aging the two catalysts above 800 °C, $BaCeO_3$ and $BaAl_2O_4$ were formed, which are believed to be detrimental for NO_x storage. Nevertheless, these undesired species could be decomposed in H_2O, NO_2, and CO_2 containing atmosphere, and the decomposition of $BaCeO_3$ was more facile than $BaAl_2O_4$, making CeO_2 a more favorable support. Recently, a high surface area Pt/Ba/CeO_2 catalyst was prepared, showing higher sulfur tolerance than the Al_2O_3 based one [23].

Thus, CeO_2 is considered to be a promising component in NSR catalysts. However, most of the previous studies focused on the structure characterization or NO_x storage capacity testing of the catalyst [12–19], without considering both lean and rich stages of NSR process. As more emphasis has been paid on the reduction process of typical NSR catalyst, we tried to give a realistic evaluation of catalytic behavior for ceria supported catalysts by using different reductants. Our aim is to further confirm the limiting steps and find the related restriction reasons during both the storage and reduction process over Pt/Ba/CeO_2 catalyst. In the present study, a transient flow reactor system was employed to evaluate the performance of Pt/Ba/CeO_2 for NO_x storage and reduction. To better understand the fundamental surface chemistry involved during lean/rich periods, dynamic DRIFTS experiments were conducted by detecting the evolution of adsorbed surface species during the NO_x storage and reduction process.

2. Experimental

2.1. Catalysts preparation

The CeO_2 supports were prepared by a precipitation method. Typically, NH_4HCO_3 aqueous solution (1 mol L^{-1}) was dropped into the $Ce(NO_3)_3$ aqueous solution (1 mol L^{-1}) and kept at pH 9–10. The obtained slurry was heated to 70 °C and stirred for 3 h. The sample was then dried at 120 °C and calcined at 500 °C in air for 3 h. The CeO_2 supported Pt/Ba catalysts were synthesized by the incipient wetness impregnation method. In brief, the CeO_2 support was impregnated with a $Ba(CH_3COO)_2$ solution, and Pt was subsequently added to Ba/CeO_2 by the same procedure using $PtCl_4$ as a precursor. After each impregnation, the samples were dried overnight at 120 °C and further calcined in air at 500 °C for 3 h. The nominal Ba and Pt loading were 20 wt% and 1 wt% respectively. The prepared catalysts were then sieved to 20–40 mesh before catalytic measurements.

2.2. Catalysts characterization

X-ray diffraction (XRD) patterns of the powder catalyst were recorded on Bruker D8 Discover (60 kV, 50 mA). The instrument was operated in step mode between 10° and 90° 2θ with a scan speed of 4°/min. Surface area and pore volume were determined by nitrogen adsorption–desorption isotherms at −196 °C over the whole range of relative pressures using a Quantasorb-18 automatic equipment (Quanta Chrome Instrument Co.). Prior to the measurement, the catalyst was outgassed at 300 °C under vacuum for 4 h.

The dispersion of Pt was determined by a H_2–O_2 titration method using a homemade pulse flow system equipped with a computer-interfaced quadruple mass spectrometer (Hiden HPR 20). Prior to H_2–O_2 titration, 100 mg of the sample was reduced in 5 vol% H_2/Ar (40 cm^3/min, 10 °C/min) at 450 °C for 1 h. The He gas (40 cm^3/min) was then passed through the sample for 1 h. After cooling to room temperature in He, the O_2 adsorption experiment was conducted, followed by flushing with He and then the introduction of H_2 pulses (1 cm^3 of 5 vol% H_2/Ar). The stoichiometries of H/Pt = 3 were assumed.

2.3. Cyclic NO_x storage reduction tests

The NSR cyclic measurements were conducted with 100 mg catalysts using a fixed-bed quartz micro-reactor with the inside diameter of 4 mm. The reactor was connected to a pneumatically actuated four-way valve, which allowed for quick switching between lean and rich atmospheres. All gases were carefully introduced by mass flow controllers with a total flow rate of 300 cm^3/min, giving a space velocity of 90,000 h^{-1}. The outlet NO_x ($NO + NO_2$) concentration was monitored by a chemiluminescence detector (ECO Physics CLD 62). The reactor was also equipped with a bypass line to ensure inlet gas concentration.

It has been reported that Pt is more likely to be in its oxidative state on ceria due to the high oxygen storage ability of ceria [20], while metallic Pt is supposed to be the active site for NO oxidation and reduction. Therefore, a H_2 reduction pretreatment is proposed to reactivate Pt sites before the NSR experiment [20]. In our study, the catalysts were pre-reduced in 1% H_2/N_2 at 450 °C for 30 min, and then exposed to rich atmosphere before stable testing temperatures were reached (200, 300, and 400 °C). The ability of NO to oxidize to NO_2 was evaluated under a steady state after the catalyst was saturated by NO/O_2. The cycling experiments were conducted with a lean period of 67 s and a rich period of 33 s. Constant flows of 500 ppm NO with either 8% O_2 or 5000 ppm H_2, or 5000 ppm CO or 556 ppm C_3H_6 (with the same molar reduction capacity) were introduced alternately during each cycle. The evolution of H_2, CO and C_3H_6 were monitored by quadruple mass spectrometer (Hiden HPR 20). Approximately 2% water vapor was added to the gas flow when required. Fifteen lean/rich cycles were carried out and average NO_x conversion was calculated according to the following formula:

$$NO_x \quad \text{conversion} = \frac{NO_{x,in} - NO_{x,out}}{NO_{x,in}} \times 100\% \tag{1}$$

The reaction byproducts of NH_3 and N_2O were measured by IR gas cell. The concentration of these byproducts were relatively low (lower than 10 ppm) due to the low concentration reductant used (0.5% H_2 or CO), thus detailed selectivity were not reported here.

2.4. In situ DRIFTS study of NO_x storage and reduction

In situ DRIFTS was performed on a Nexus 670 (Thermo Nicolet) FTIR spectrometer equipped with an *in situ* diffuse reflection chamber and a high-sensitivity MCT detector. The catalyst for the *in situ* DRIFTS studies was finely ground and placed in a ceramic crucible in the *in situ* chamber. Mass flow controllers and a sample temperature controller were used to maintain an atmosphere identical to the catalytic activity tests. To separate multiple reactions during the complicated NO_x storage and reduction process and allow for easy study, the lean/rich period were prolonged to 60 min and 30 min. Prior to recording DRIFT spectra, the catalyst was pretreated in 20% O_2/N_2 for 30 min at 450 °C, and then another 30 min reduction in 1% H_2 at the same temperature. After pretreatment, the catalysts were purged with N_2 and cooled to the desired temperature (200, 300, 400 °C) to acquire a reference spectrum. After that, the catalysts were exposed to a mixture of 500 ppm NO and 8% O_2 and a series of NO_x adsorption spectra over time were collected. After adsorption for an hour, the gas flow was switched to the reducing agent. Either 5000 ppm H_2 or 5000 ppm CO or 556 ppm C_3H_6 balanced with N_2 was used. All spectra reported here were collected at a resolution of 4 cm^{-1}.

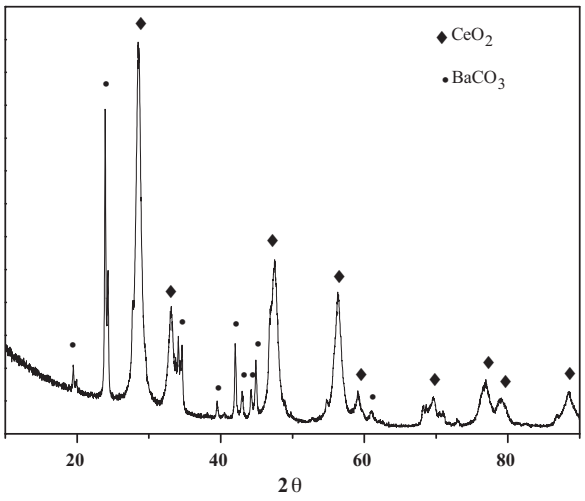

Fig. 1. XRD patterns of $Pt/Ba/CeO_2$ catalyst.

3. Results and discussion

3.1. Characterization results

Fig. 1 shows the XRD spectra of fresh $Pt/Ba/CeO_2$ catalysts. Obviously, the CeO_2 support exhibited a typical cubic fluorite structure (JCPDS No. 810792). The deposited Ba on the catalysts was mainly in the form of crystalline $BaCO_3$ (JCPDS No. 71-2394). This is in agreement with previous reports that BaO could be easily transformed to carbonate in the presence of air [24]. The reflection of Pt could not be observed due to its low content or its high dispersion on the catalyst. Pure CeO_2 had a surface area of 84.0 m^2/g. As Ba and Pt were sequentially added, the surface area of $Pt/Ba/CeO_2$ decreased to 44.1 m^2/g. The dispersion of Pt was estimated to 45%.

Table 1
The outlet concentrations of NO, NO_2, NO_x after $Pt/Ba/CeO_2$ were saturated by NO_x.

Temperature	NO	NO_2	NO_x	NO_2/NO_x (%)
200	493	5	498	0.1
300	458	35	493	7
400	254	238	492	48

3.2. NO_x storage and reduction by H_2

Fig. 2a–c depicts the evolutions of NO_x in the outlet feed of the initial fifteen lean/rich cycles by using H_2 as reductant at 200, 300 and 400 °C, respectively. Fig. 2d summarizes the average conversions of these cycles at each temperature. As seen in Fig. 2a (200 °C), a significant amount of NO_x broke through before the end of the storage period, and the outlet NO_x concentration at the lean phase gradually steadied at around 220 ppm with continuing cycles. This indicates that NO_x was not completely trapped on the catalysts during the 67 s storage duration. Table 1 showed the outlet concentration of NO, NO_2 and NO_x when the catalyst was saturated by NO_x, representing NO oxidation ability. The NO conversion to NO_2 was as low as 0.1%, which may account for the limited storage capacity of the catalyst at this temperature considering that NO_2 could be more effectively trapped than NO [25,26]. When the gas flow was subsequently switched to the rich atmosphere, a great spike appeared and then quickly decreased to zero. This spike has been commonly observed in previous research [13,27], and was caused by different initial rates between nitrates decomposition and released NO_x reduction. Obviously, the NSR performance at this temperature was limited by the storage process but not the release

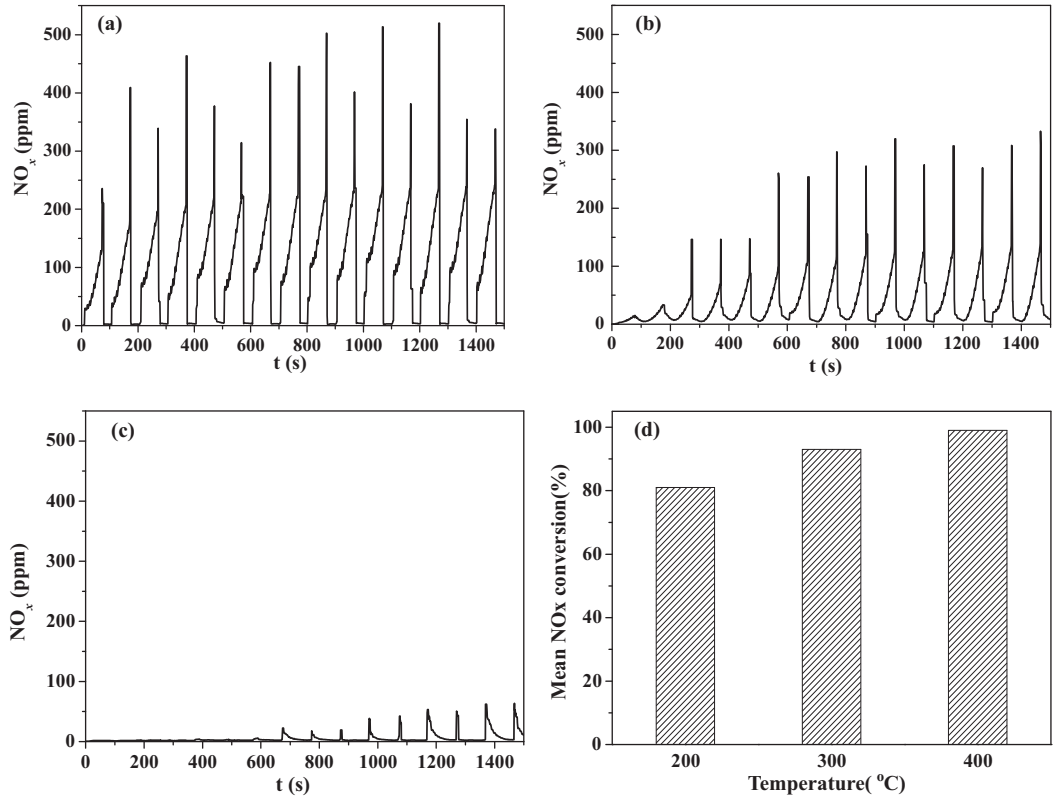

Fig. 2. Evolutions of NO_x concentrations under cyclic lean-rich conditions with H_2 as reductant over $Pt/Ba/CeO_2$ at 200 °C (a), 300 °C (b), 400 °C (c). Part (d) summarized the average NO_x conversion of each temperature. Lean (67 s): 500 ppm NO, 8% O_2, N_2 balanced; rich (33 s): 500 ppm NO, 0.5% H_2, N_2 balanced.

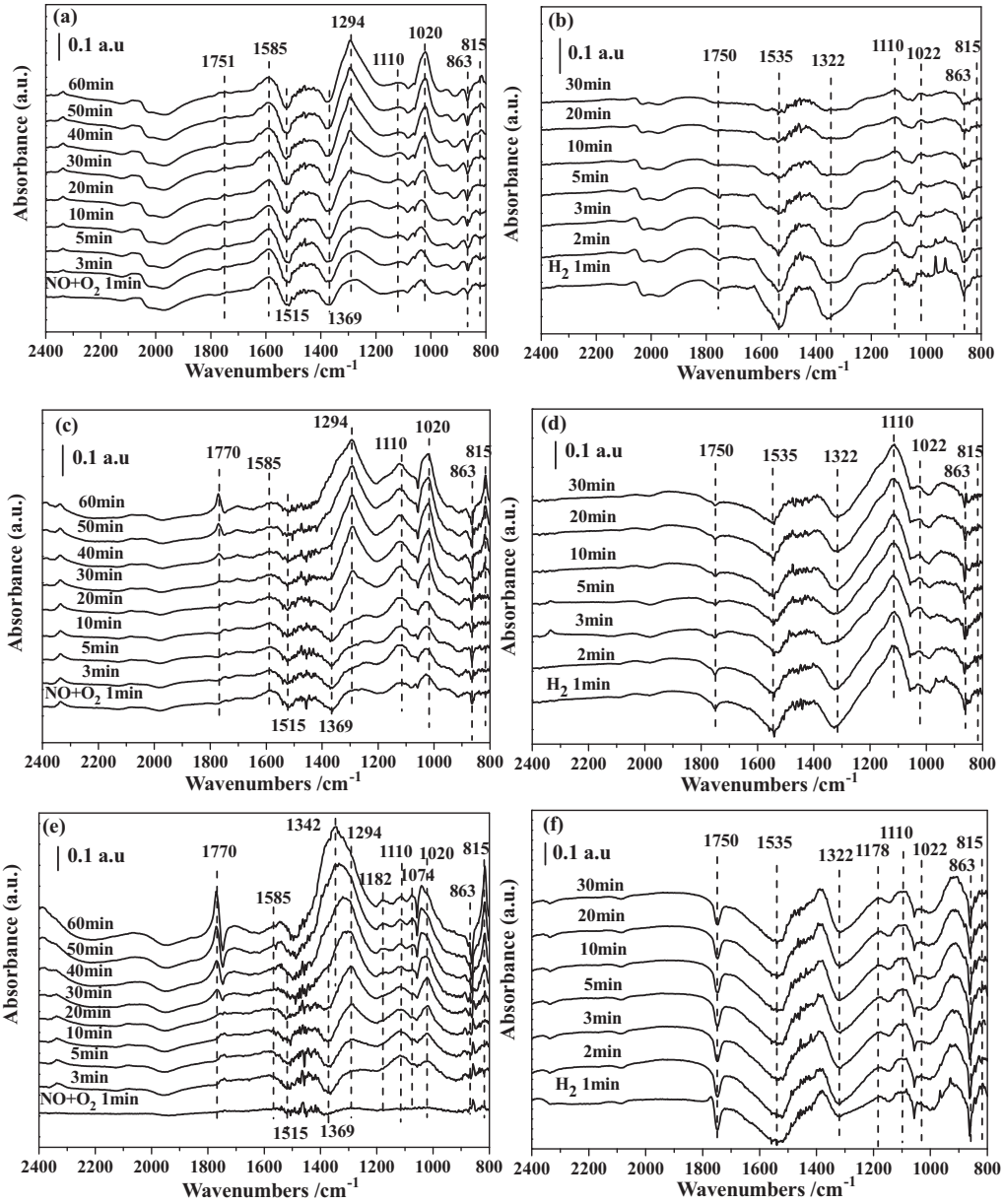

Fig. 3. In-situ DRIFT spectra of storage and reduction processes over $Pt/Ba/CeO_2$ using H_2 as reductant. Parts (a), (c) and (e) represented the storage process at 200 °C, 300 °C, 400 °C; (b), (d) and (f) represented the reduction process at 200 °C, 300 °C, 400 °C.

or reduction. As cyclic NSR performance is determined by the co-effect of lean and rich stages, average NO_x conversion during the fifteen cycles was used to describe the NO_x removal efficiency. By using H_2 as the reductant at 200 °C, average NO_x conversion of 81% and H_2 conversion of 75% were obtained. The consumption of H_2 was about 26% higher than that required to reduce NO_x, which could be attributed to the consumption of oxygen whether released from the catalyst or residual in the gas phase when transited from lean to rich. When the temperature was increased to 300 °C, the outlet NO_x breakthrough decreased significantly to only 20 ppm during the first cycle. With continuing cycles, however, more NO_x spilled out and its concentration gradually steadied to around 100 ppm at the end of the lean durations. The improved NO_x storage capacity at 300 °C compared with 200 °C was attributed to an increase in NO oxidation ability at this temperature (ca. 7%). The deactivation of the first several cycles may relate to increased nitrates stability but less H_2 reductive ability towards certain ad-NO_x species. Fifteen cycles gave an average NO_x conversion of 93% at 300 °C, and the conversion of H_2 increased to 97% due to the increased NO_x reduction ability and oxygen storage capacity of the catalyst. The consumption of H_2 by oxygen (residual or released) accounts for 42% of the total. By increasing the temperature to 400 °C, both the lean NO_x breakthrough and transition spikes were greatly reduced and the average NO_x conversion reached 99%. This improvement was likely due to the increased NO to NO_2 conversion (ca. 48%) and the high reactivity of H_2 towards ad-NO_x reduction with temperature increases. The storage sites during the preceding lean phase could be fully regenerated, thus leading to complete adsorption of NO_x during subsequent cycles. Moreover, the consumption of H_2 was nearly 100% at this temperature and that used for oxygen oxidation accounts for 40%. For comparison, the NO_x removal efficiency of $Pt/Ba/Al_2O_3$ was also tested under the same reaction condition, with NO_x conversions of 90%, 95%, 92% at 200, 300, 400 °C, respectively. Obviously, the best performance of $Pt/Ba/Al_2O_3$ was around 300 °C, while $Pt/Ba/CeO_2$ performed well around 400 °C. The relative low activity of $Pt/Ba/CeO_2$ at low temperatures compared with

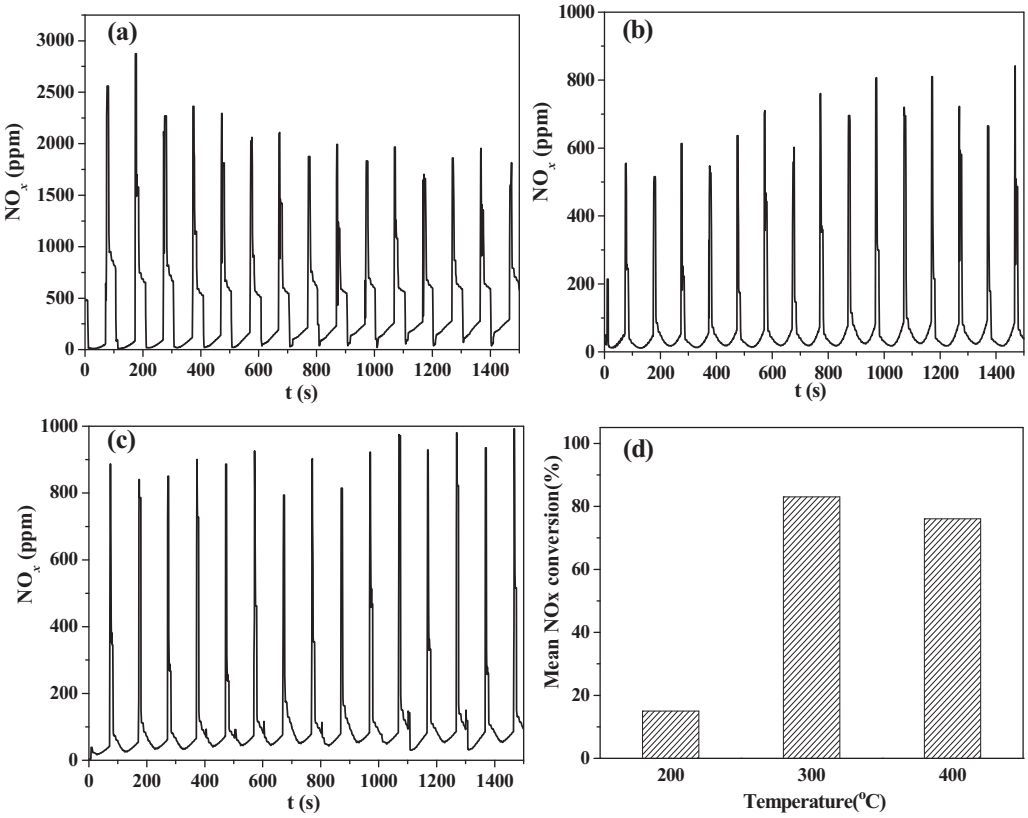

Fig. 4. Evolutions of NO_x concentrations under cyclic lean-rich conditions with CO as reductant over $Pt/Ba/CeO_2$ at 200 °C (a), 300 °C (b), 400 °C (c). Part (d) summarized the average NO_x conversion of each temperature. Lean (67 s): 500 ppm NO, 8% O_2, N_2 balanced; rich (33 s): 500 ppm NO, 0.5% CO, N_2 balanced.

$Pt/Ba/Al_2O_3$ may be ascribed to the relatively low surface areas (44.1 m^2/g vs. 217.7 m^2/g), the different dispersions of Pt and Ba as well as the nitrates stability, which need a further investigation in following work. We also noticed that the H_2 consumption of $Pt/Ba/Al_2O_3$ was about 10% lower than that of $Pt/Ba/CeO_2$, which had a connection with the increased oxygen storage capacity of ceria compared with alumina.

The corresponding DRIFT spectra during the course of NO_x storage and reduction (with H_2) are presented in Fig. 3. The NO_x storage profiles as a function of time at different temperatures are shown in Fig. 3a, c and e. Specific absorption bands and their assignments were listed in Table 2. As NO and O_2 were introduced over the catalysts at 200 °C (Fig. 3a), the bidentate nitrates on barium sites (1585, 1294, and 1020 cm^{-1}) formed quickly. Specifically, the bands at 1020 and 1294 cm^{-1} were assigned to the symmetric and asymmetric stretching mode of $-NO_2$, and the band at 1585 cm^{-1} was characteristic of N=O vibration [6,28]. Another significant band at 1110 cm^{-1} could be assigned to nitrates species on ceria [29]. Along with the formation of nitrates, two negative bands centered at 1515 and 1369 cm^{-1} also appeared and were attributed to the decomposition of surface barium carbonates as barium carbonates were the major form present before the background spectrum was collected [6,30]. The NO_x storage profiles indicate that barium nitrates were formed by replacing carbonate species on the catalyst surface, and this kind of carbonates was supposed to be LT-$BaCO_3$, which were active in NO_x storage [19]. Previous studies have demonstrated that the decarbonisation of barium carbonates under the effect of NO_2 was thermodynamically favorable even at room temperature [30]. With time, the originally formed nitrate bands became more intense. Additionally, weak bands around 1751 and 815 cm^{-1} became distinct at the end of storage. Roedel et al. [31] assigned these two bands as bulk nitrates associated with barium by different IR techniques. The band at 1751 cm^{-1} was ascribed to the combination mode ($\nu_1 + \nu_4$) of nitrate and the band at 815 cm^{-1} to the ν_2 mode. According to this NO_x storage feature, it is easy to infer that surface nitrates gradually diffused into the bulk of the catalyst with a continuous flowing lean stream. In addition, no evident intermediate species such as nitrites were observed during the entire storage process. However, the formation of nitrites has been widely reported on $Pt/Ba/Al_2O_3$ catalysts and has been considered an important pathway for NO_x adsorption [32–34]. Urakawa et al. [35] also detected nitrites formation at the location of 1204 cm^{-1} on the surface of $Pt/Ba/CeO_2$ by time-resolved DRIFTS. For the ceria supported catalysts in the present study, we assumed that bands of nitrite may be overlapped by the fast growing bands of nitrates or nitrites quickly transformed to nitrates.

The impact of temperature on the features of surface species during the lean phase was also speculated on. Obviously, the final intensities of nitrate peaks (1294, 1110, and 1020 cm^{-1}) at 300 °C (Fig. 3c) were stronger than those at 200 °C (Fig. 3a), indicating more trapping sites (both Ba and Ce) were utilized at elevated

Table 2
Summary of the DRIFT spectral assignments.

Wavenumber (cm^{-1})	Assignments	Associated phase	Reference
1585, 1294, 1020	Bidentate nitrate	Ba	[6,30]
1751, 1770, 815, 1342	Bulk nitrate	Ba	[31,34,36]
1182, 1110, 1074	Nitrate	Ce	[29,37]
1500–1600	Carbonate	Ba	[30,31,38,39,41]
1300–1400			
863			
2057	Carbonyl (-CO)	Pt	[30,36]
2175, 2121	Gas phase CO	–	[42]

temperature. This result was consistent with the former transient flow reactor test in Fig. 2, and was attributed to the increased NO oxidation ability of $Pt/Ba/CeO_2$ at 300 °C. When the temperature increased to 400 °C, nitrate bands became even more distinct. After NO_x storage for 60 min over $Pt/Ba/CeO_2$ at this temperature, the main nitrate band at 1294 cm^{-1} shifted to 1342 cm^{-1}. This transformation was caused by the increasing coverage of nitrate species and the formation of bulk nitrates [34,36]. It also should be noted that bands at 1751/1770 and 815 cm^{-1}, which were previously ascribed to bulk barium nitrates, increased significantly with temperature (200–400 °C). In addition, two bands at 1182 and 1074 cm^{-1} became apparent at 400 °C. These new bands appeared only at high temperature and long exposure to NO_x/O_2 atmosphere, and they might be assigned to bulky ceria nitrates by comparing with the NO_x adsorption feature on pure ceria [37]. All these features support the fact that increasing temperature accelerated surface nitrates formation as well as diffusion into bulk of the catalyst.

As the gas flow was switched to the reductive atmosphere of H_2, the NO_x reduction efficiencies were significantly high for all tested temperatures. As seen in Fig. 3b, d and f, the $Ba(NO_3)_2$ bands (1770, 1585, 1294, 1020, and 815 cm^{-1}) quickly disappeared as soon as H_2 was introduced. Simultaneously, two broad negative bands at 1535 and 1322 cm^{-1} and two small negative bands at 1750 and 863 cm^{-1} appeared, originating from the decomposition of carbonates [30,31,38,39]. Based on this phenomenon, the negative bands could be an indication of nitrates decomposition or reduction during the rich period. Though we have observed decarbonisation during the storage period, this feature was not so apparent due to partial overlapping by the formation of nitrates species. With nitrates decomposition and no carbon-containing species formation during the rich period, the negative peaks dominated the reduction spectra. By comparing the intensities of negative peaks at different temperatures, the amount of $BaCO_3$ involved in the NSR process could be identified. Clearly, the negative bands at 400 °C were more intense than those at 300 °C and 200 °C due to larger replacement of carbonates at the lean phase. These results were in agreement with the $Ba(NO_3)_2$ accumulation features observed in Fig. 3a, c and e. Furthermore, we also noted that most nitrate species were removed as soon as the reductant was introduced, however, some residual nitrates located on Ce sites (1110 cm^{-1}) were still present even after 30 min reduction. Therefore, H_2 appeared more reactive towards $Ba(NO_3)_2$ reduction than $Ce(NO_3)_4$ reduction. The remaining cerium nitrate at 300 °C was more predominant than at 200 °C, which is probably due to the increased NO_x capture ability on Ce sites but relatively low reduction effect towards $Ce(NO_3)_4$ at this temperature. This provided additional evidence for the deactivation of the initial cycling performance in Fig. 2b, which suggested decreased trapping capacity may arise from un-released cerium nitrate. The reduction process at 400 °C was much improved as evidenced by the disappearance of both $Ba(NO_3)_2$ and $Ce(NO_3)_4$ bands.

According the detailed DRIFTS analysis and cyclic experiment above, several main points were obtained:

1) During the lean period, NO_x can be adsorbed on both Ba and Ce sites by replacing carbonates species, and the storage capacity increased as a function of temperature from 200 to 400 °C.
2) During the rich period, H_2 regenerated the surface quickly, $Ba(NO_3)_2$ could be easier reduced than $Ce(NO_3)_4$.
3) When using H_2 as the reductant, the cyclic NO_x storage and reduction performance was limited by NO oxidation and sorption at low temperatures.

3.3. NO_x storage and reduction by CO

Fig. 4a–c shows the outlet NO_x concentration over $Pt/Ba/CeO_2$ during the fifteen consecutive lean/rich cycles at 200, 300 and

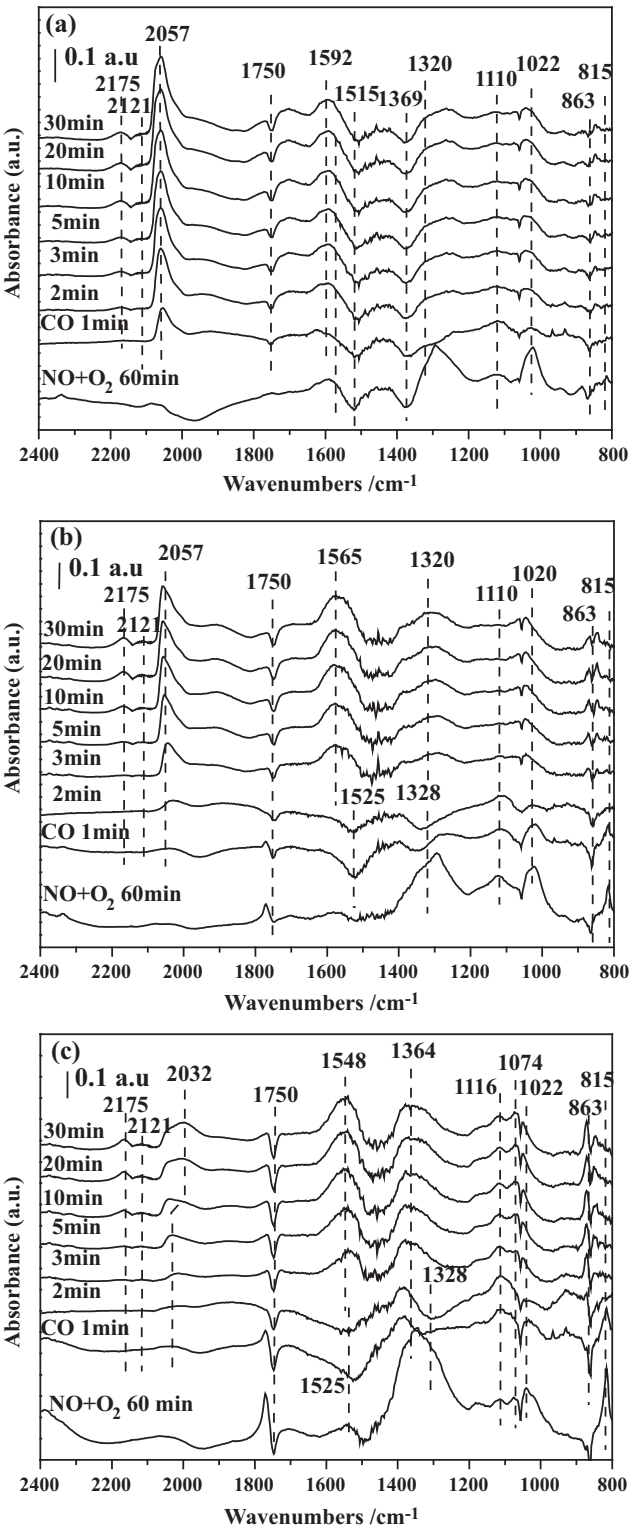

Fig. 5. In-situ DRIFT spectra of storage and reduction processes over $Pt/Ba/CeO_2$ using CO as reductant. Parts (a)–(c) represented the reduction process at 200 °C, 300 °C, 400 °C.

400 °C using CO as the reductant. As seen in Fig. 4a (200 °C), the catalyst exhibited similar NSC during the first cycle as that in Fig. 2a. Nevertheless, the reduction efficiency was greatly deteriorated when using CO compared with H_2. The maximum NO_x concentration reached as high as 3000 ppm during transition from lean to rich atmosphere at 200 °C, demonstrating a relatively high releas-

ing rate of ad-NO_x when exposed to rich atmosphere. Subsequently, the emitted NO_x decreased due to the reduction performance of CO, although the reduction effect was rather poor. A "step-like" feature during the rich phase represented the low NO_x reduction efficiency at this temperature. Only when the next lean cycle began, did the NO_x concentration at the end of reduction phase decrease sharply due to the trapping effect of the relaxed storage sites. It seems that CO could facilitate $Ba(NO_3)_2$ decomposition but not NO_x reduction, unlike H_2 which could accelerate both steps. A similar conclusion was obtained by James et al. [40]. In the present study, the low regeneration efficiency of CO led to gradually decreasing NO_x trapping performance of subsequent cycles. As a result, an average NO_x conversion of 15% was obtained. When the temperature increased to 300 °C (Fig. 4b), the cycle-averaged NO_x conversion was significantly improved to 83%. This promising effect could be attributed to both increased NO_x storage and reduction efficiencies. However, the NO_x conversion at 400 °C decreased to 76%. This decline was connected with decreased NSC at this temperature, as illustrated by the incomplete NO_x storage feature in Fig. 4c. One possible reason for this is that the reaction product of carbonates accumulated on the catalysts, which influenced further decomposition of nitrates and thus NO_x adsorption of subsequent cycles. This assumption was further confirmed by later DRIFTS experiments. The conversions of CO were 35%, 94%, 98% at 200, 300, 400 °C, respectively. The consumption of CO was attributed to both the reduction of NO_x as well as oxygen.

As DRIFT spectra of the NO_x storage process were similar to those in Fig. 3, Fig. 5 shows the corresponding NO_x reduction process over the $Pt/Ba/CeO_2$ sample using CO as the reductant. When the feed was switched to CO at 200 °C (Fig. 5a), the previously formed barium nitrates bands (1585, 1294, and 1022 cm^{-1}) decreased immediately. However, the reduction feature of the nitrates peaks seemed less prominent when using CO compared to the similar reduction process using H_2 in Fig. 3b (assuming both cases have the same accumulated nitrates amount at lean phase). This may be due to the reaction products of barium carbonates being formed simultaneously with nitrates decomposition on the catalyst surface. Consequently, the surface species comprised a mixture of newly formed carbonates and unreleased nitrates. As the DRIFT spectra of carbonates partially overlapped with nitrates, the gradually growing bands around 1592 cm^{-1} and 1320 cm^{-1} were tentatively ascribed to newly formed carbonates [41]. The location of these carbonate species deviated somewhat from those replaced by NO_x during the storage process (negative peaks at 1535 and 1322 cm^{-1}). This may be attributed to the strong influence of unreleased nitrates (especially the nitrate band at 1585 cm^{-1}). The reduction efficiencies at 300 and 400 °C were much more improved. As demonstrated in Fig. 5b and c, two widened negative bands at 1525 and 1328 cm^{-1} appeared during the initial reduction stages, indicating the effective release of adsorbed NO_x. Subsequently, the negative peaks were overlapped by growing carbonate bands at 1600–1500 cm^{-1} and 1400–1300 cm^{-1}. In the reduction process, the carbonate band at 1592 cm^{-1} gradually shifted to 1548 cm^{-1} when the temperature increased from 200 °C to 400 °C. This mostly can be ascribed to the lesser overlapping feature of nitrates bands and carbonates bands, which arose from the improved reaction of released NO_x with CO at higher temperatures. In addition, by observing the decreased cerium nitrate band at 1110 cm^{-1}, CO was more reactive towards $Ce(NO_3)_4$ reduction than H_2.

During the process of NO_x reduction by CO at 200 and 300 °C, a strong band at 2057 cm^{-1} was observed and assigned to the linear bonded CO over Pt site [30,36]. Two small peaks centered at 2175 and 2121 cm^{-1} were related to gaseous CO [42]. The intensities of both species increased as a function of time at all temperature

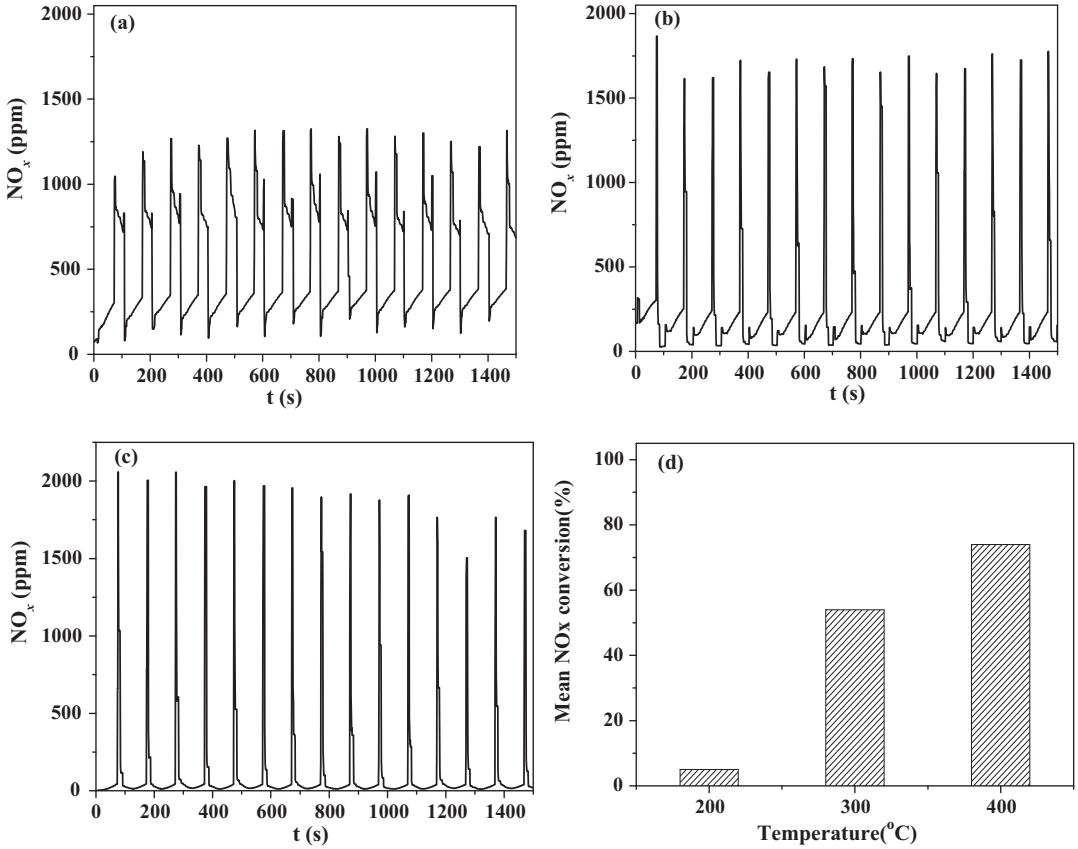

Fig. 6. Evolutions of NO_x concentrations under cyclic lean-rich conditions with C_3H_6 as reductant over $Pt/Ba/CeO_2$ at 200 °C (a), 300 °C (b), 400 °C (c). Part (d) summarized the average NO_x conversion of each temperature. Lean (67 s): 500 ppm NO, 8% O_2, N_2 balanced; rich (33 s): 500 ppm NO, 556 ppm C_3H_6, N_2 balanced.

ranges, and reached a maximum at the end of the reduction. The Pt–CO species have been commonly found on the $Pt/Ba/Al_2O_3$ catalyst when using CO as a reducing agent, and have a strong influence on NSR performance [30,38,43]. Specifically, in a typical NSR process, Pt plays an important role in NO oxidation and reduction. However, when using CO as the reductant, some Pt sites were occupied by CO species, resulting in a decrease in active sites available for NO or reductant adsorption/dissociation, thus directly deteriorating storage and regeneration performances.

Temperature also impacted the poison extent of Pt. As shown in Fig. 5, the band at 2057 cm^{-1} appeared when exposing $Pt/Ba/CeO_2$ to CO for 1 min at 200 °C, while this band became evident after 3 or 5 min under CO exposure at 300 and 400 °C. This indicates that the formation of linear Pt–CO was rather fast at low temperature, and that the Pt–CO band intensity weakened with increasing temperature. The changes to the Pt–CO band partially explained the activity changes in the transient flow reactions in Fig. 4. The low NO_x conversion at 200 °C was due to the less reductive ability of CO compared with H_2 and its serious poison effect on Pt sites. At 300 °C, the reduction ability of $Pt/Ba/CeO_2$ was improved due to less Pt–CO interaction. However, the decreased NO_x conversion at 400 °C could not be explained by the release of active sites of Pt only. Though the poison extent of Pt by CO adsorption lessened at this temperature compared with 300 °C, other influencing factors involved in the cyclic operation deteriorated the whole performance. As is known, the reduction process with CO is supposed to function according to the reaction $5CO + Ba(NO_3)_2 \rightarrow BaCO_3 + N_2 + 4CO_2$. Ji et al. suggested that the formation of a crust of carbonates may block further decomposition of nitrates in a rich atmosphere [44]. We also observed increased carbonates coverage at 400 °C (Fig. 5c). Therefore, in combination with the DRIFTS experiments and transient flow reactions, the inferior NO_x removal efficiency of CO compared with H_2 over the $Pt/Ba/CeO_2$ catalyst was further clarified. Low NO_x removal efficiency at 200 °C was attributed to CO poison to the surface Pt sites, while decreased NSR performance at 400 °C was related to the negative effect of accumulated carbonates on the catalyst.

3.4. NO_x storage and reduction by C_3H_6

Fig. 6 shows the results of the NSR experiment using C_3H_6 as the reducing agent between 200 and 400 °C. At 200 °C (Fig. 6a), the NO_x removal performance was rather poor with a conversion of less than 5%. When the temperature was increased to 300 °C (Fig. 6b), the average NO_x conversion increased to 54%. This improvement was connected with increased reduction efficiency of C_3H_6 and somewhat increased storage capacity. When the temperature was increased to 400 °C, the NO_x breakthrough concentration during the lean phase (Fig. 6c) was greatly reduced, indicating more effective NO_x storage at this temperature. This mostly can be attributed to the easy activation of C_3H_6 at elevated temperature, inducing a more profound regeneration of storage sites. Finally, about 74% of the NO_x conversion was obtained at 400 °C. The consumptions of C_3H_6 were 27%, 76%, 95% at 200, 300, 400 °C, respectively.

The dynamic change of corresponding DRIFT spectra of $Pt/Ba/CeO_2$ in flowing C_3H_6 atmosphere at different temperatures are shown in Fig. 7. Upon exposure of the catalysts to C_3H_6 at 200 °C, the nitrates formed during the storage process decreased quickly with time, as manifested by the negative bands at 1750, 1586, and 1294 cm^{-1} in DRIFT spectra. This feature indicated the decomposition of adsorbed NO_x. However, no obvious reaction products of carbonates were observed during the initial 10 min reduction at 200 °C. Only when the reduction process lasted more than 20 min were the negative bands gradually covered by growing bands around 1586 and 1300 cm^{-1}, indicating slow carbonates formation. These results were in accordance with the gas-phase

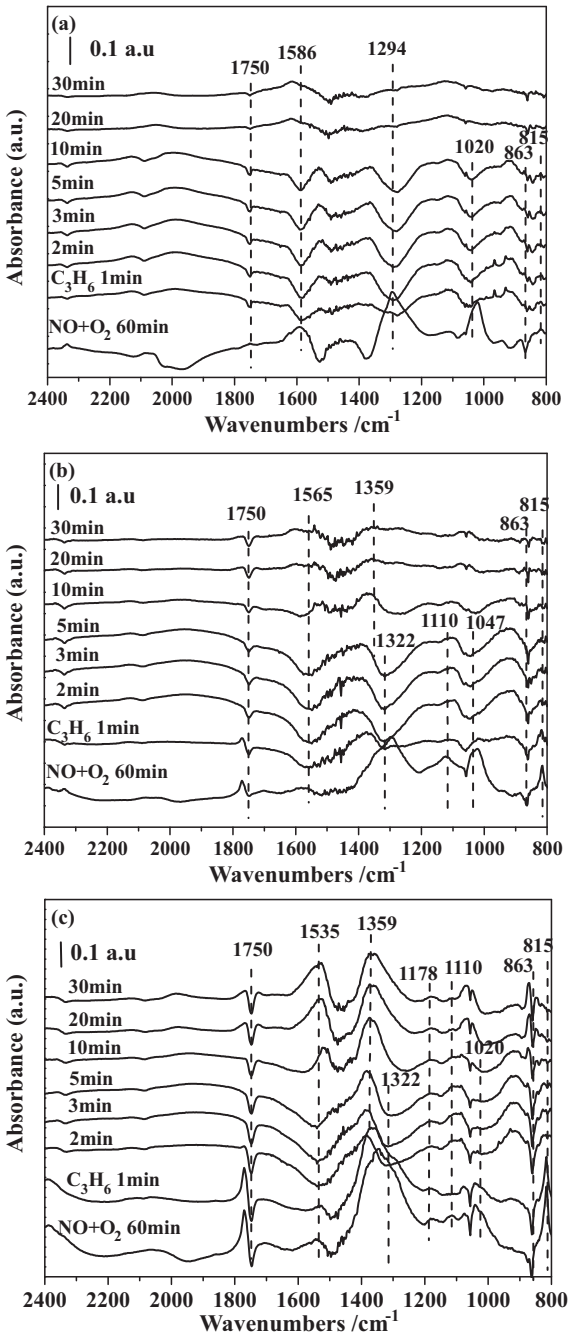

Fig. 7. In-situ DRIFT spectra of storage and reduction processes over $Pt/Ba/CeO_2$ using C_3H_6 as reductant. Parts (a)–(c) represented the reduction process at 200 °C, 300 °C, 400 °C.

reaction listed in Fig. 6a, which suggested only a small amount of the released NO_x was reduced by C_3H_6 at 200 °C during the reduction period, thus resulting in relatively low coverage of surface carbonates. With increasing temperature, the reduction efficiency of C_3H_6 improved. As illustrated in Fig. 7b, the negative bands at 1565 and 1322 cm^{-1} became apparent during the initial 5 min reduction, suggesting more $Ba(NO_3)_2$ were decomposed from the catalysts. The released NO_x showed an improved reaction with gaseous C_3H_6 as evidenced by gas-phase reaction in Fig. 6b. Accordingly, carbonates accumulation (1565 and 1359 cm^{-1}) became apparent after 10 min reduction in FTIR spectra. Reduction at 400 °C showed a much similar feature to that at 300 °C, and the bands of carbonates at 1535 and 1359 cm^{-1} exhibited much higher intensities due to increased

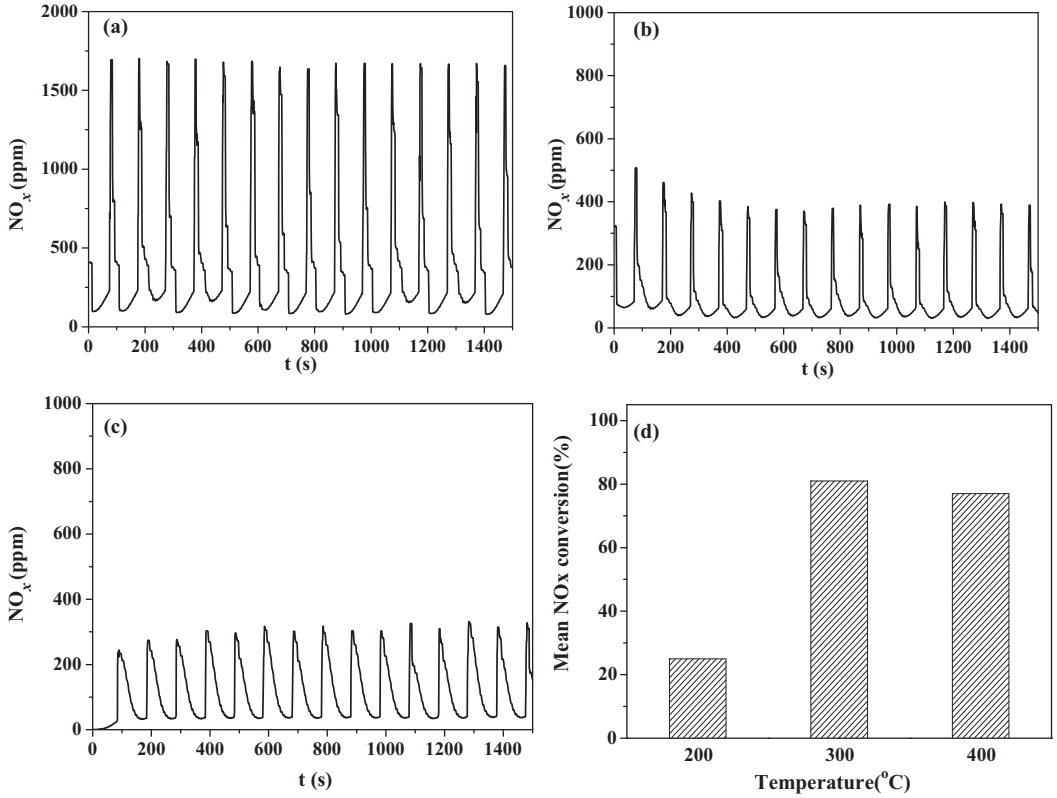

Fig. 8. Evolutions of NO_x concentrations under cyclic lean-rich conditions with water addition using CO as reductant over $Pt/Ba/CeO_2$ at 200 °C (a), 300 °C (b), 400 °C (c). Part (d) summarized the average NO_x conversion of each temperature. Lean (67 s): 500 ppm NO, 8% O_2, 2% H_2O, N_2 balanced; rich (33 s): 500 ppm NO, 0.5% CO, 2% H_2O, N_2 balanced.

reduction efficiency of C_3H_6. The negative effect of reaction products (carbonates) may also exist in the NSR process as that described in the case of CO reduction. However, it was the nature of propene that determined the whole NO_x removal efficiency over $Pt/Ba/CeO_2$ in transient flow reactors. C_3H_6 was more difficult to be activated than H_2 and CO, which resulted in relatively low NO_x reduction performance during all tested temperatures.

3.5. Water addition effect on CO reduction process

According to the above experiments, H_2 was evidenced to be the most effective reductant among H_2, CO, and C_3H_6 over $Pt/Ba/CeO_2$ catalyst. It has also been reported that Pt/CeO_2 is a good water gas shift catalyst [9]. Considering that exhaust gas usually contains a significant amount of steam, a WGS reaction may occur on $Pt/Ba/CeO_2$. Therefore, the impact of H_2O on NO_x storage reduction system was studied using CO as the reductant. The transient flow reactor results are depicted in Fig. 8. With the addition of water, a decrease in NO_x storage capacity during the lean period was observed, illustrated by the early NO_x breakthrough and higher concentration at the end of storage. The negative effect of H_2O towards NO_x storage has been reported on a $Pt/Ba/Al_2O_3$ system and is considered to be due to the competitive adsorption of NO_x and H_2O on the storage sites [45]. The same effect may also exist in $Pt/Ba/CeO_2$. During the reduction period, the outlet NO_x concentration showed a decrease in NO_x spikes compared with no water addition during all tested temperatures (Fig. 4). In the presence of water, the average NO_x conversion was 27% at 200 °C, which was about 10% higher than without water. The NO_x conversions at 300 and 400 °C were 82% and 77%, respectively, which were very similar to results in Fig. 4, with little improvement in total NO_x conversion when water was present. At higher temperatures, the impact of H_2O on NO_x storage is supposed to be less important than that on low temperatures [17]; however, no obvious improvement in NO_x conversion at 400 °C may be connected with the increased activity of CO towards NO_x reduction. WGS reaction plays a minor role in NSR reduction process over $Pt/Ba/CeO_2$, which may have a connection with the kinetics of this reaction. Partridge et al. have shown that H_2 formation via WGS reaction is too slow to facilitate the removal of nitrates and subsequent reduction of NO_x [46].

By observing that NSR performance at 200 °C was improved in the presence of H_2O, we examined surface species evolution, especially for the poisoned Pt sites, by DRIFTS. In this study, flowing 2%

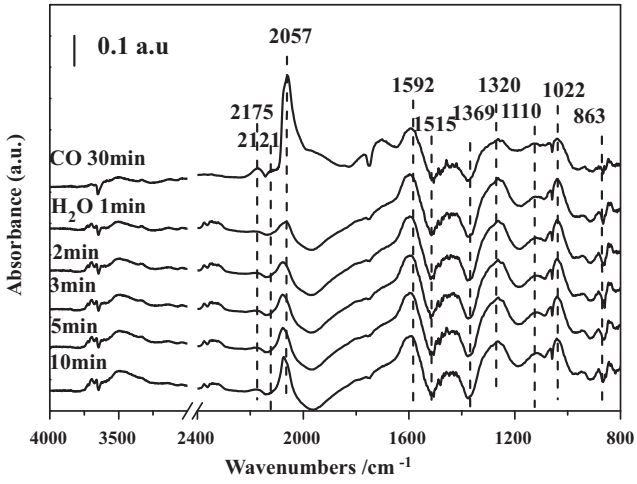

Fig. 9. Dynamic changes of *in situ* DRIFT spectra of $Pt/Ba/CeO_2$ after 2% water vapor was introduced into the feed gas of 0.5% CO/N_2 at 200 °C. Before water vapor was introduced, $Pt/Ba/CeO_2$ was undergoing the CO reduction process as that shown in Fig. 5a.

H_2O gas was added to the catalyst which had be exposed to a CO reduction atmosphere for 30 min at 200 °C (Fig. 9). After exposing the catalyst to CO for 30 min, a strong peak was observed due to CO adsorbed on Pt. However, it was greatly suppressed by water addition, especially during the initial period. Simultaneously, a band around 3500 cm^{-1} increased gradually. As a consequence, the positive effect of H_2O addition at 200 °C could mostly be ascribed to the reduced Pt–CO population.

4. Conclusion

According to comparative studies of NSR performances using H_2, CO, and C_3H_6 as the reducing agents at different temperatures, the differences in NO_x removal activities over a $Pt/Ba/CeO_2$ catalyst were further clarified. NO_x can be adsorbed on both Ba and Ce sites by replacing carbonates species, and the storage capacity increased as a function of temperature from 200 to 400 °C. NSR performance increased with increased temperature with H_2 and C_3H_6 as reductants during the temperature range 200–400 °C, while maximum NSR performance was obtained at 300 °C with CO as a reducing agent. The most prominent effect was shown by H_2, especially at low temperature, which is in accordance with previous reports. The deteriorated reduction efficiency of CO at 200 °C was due to a serious poisoning of Pt sites, while the decreased NSR performance at 400 °C was mostly attributed to the negative effect of carbonates. The least reactivity of C_3H_6 was due to its lowest activation ability by the catalysts as well as carbonates accumulation. Barium carbonates seem to play two different roles in NO_x storage reduction process. For one thing, they could participate in NO_x storage, with nitrates formation and CO_2 releasing. For another thing, the carbonates accumulated on the surface of catalysts during the reduction process by using CO and C_3H_6 as reductants, which block nitrates release as well reduction. H_2O had a positive effect in CO reduction process, which was due to the suppressed Pt–CO interaction. Simultaneously, H_2O competed with NO_x to adsorb on storage sites, which negatively influenced NO_x storage capacity. As a result, water only improved NO_x conversion at 200 °C, appearing to have little effect on total NO_x removal performances at 300 °C and 400 °C.

Acknowledgments

This work was financially supported by the National High Technology Research and Development Program of China (2007AA06Z314, 2009AA064802) and the National Basic Research Program of China (2010CB732304).

References

[1] R. Burch, Catal. Rev. 46 (2004) 271–334.
[2] W.S. Epling, L.E. Campbell, A. Yezerets, N.W. Currier, J.E. Parks, Catal. Rev. 46 (2004) 163–245.
[3] S.M.N. Miyoshi, K. Katoh, J. Harada, N. Takahashi, K. Yokota, M. Sugiura, K. Kasahara, SAE Tech. Paper 950809, 1995.
[4] N. Takahashi, H. Shinjoh, T. Iijima, T. Suzuki, K. Yamazaki, K. Yokota, H. Suzuki, N. Miyoshi, S.-i. Matsumoto, T. Tanizawa, T. Tanaka, S.-s. Tateishi, K. Kasahara, Catal. Today 27 (1996) 63–69.
[5] E. Fridell, M. Skoglundh, B. Westerberg, S. Johansson, G. Smedler, J. Catal. 183 (1999) 196–209.
[6] F. Prinetto, G. Ghiotti, I. Nova, L. Lietti, E. Tronconi, P. Forzatti, J. Phys. Chem. B (2001) 12732–12745.
[7] S.i. Matsumoto, Catal. Today 90 (2004) 183–190.
[8] Y. Nagai, T. Hirabayashi, K. Dohmae, N. Takagi, T. Minami, H. Shinjoh, S.i. Matsumoto, J. Catal. 242 (2006) 103–109.
[9] Y.T. Kim, E.D. Park, H.C. Lee, D. Lee, K.H. Lee, Appl. Catal. B 90 (2009) 45–54.
[10] G. Jacobs, U.M. Graham, E. Chenu, P.M. Patterson, A. Dozier, B.H. Davis, J. Catal. 229 (2005) 499–512.
[11] L.F. Liotta, A. Macaluso, G.E. Arena, M. Livi, G. Centi, G. Deganello, Catal. Today 75 (2002) 439–449.
[12] Y. Ji, T. Toops, M. Crocker, Catal. Lett. 119 (2007) 257–264.
[13] Y. Ji, J.-S. Choi, T.J. Toops, M. Crocker, M. Naseri, Catal. Today 136 (2008) 146–155.
[14] M. Piacentini, M. Maciejewski, A. Baiker, Appl. Catal. B 72 (2007) 105–117.
[15] V. Schmeißer, J. de Riva Pérez, U. Tuttlies, G. Eigenberger, Top. Catal. 42–43 (2007) 15–19.
[16] M. Casapu, J.-D. Grunwaldt, M. Maciejewski, A. Baiker, S. Eckhoff, U. Gobel, M. Wittrock, J. Catal. 251 (2007) 28–38.
[17] E.C. Corbos, X. Courtois, N. Bion, P. Marecot, D. Duprez, Appl. Catal. B 76 (2007) 357–367.
[18] Y.Y. Ji, T.J. Toops, M. Crocker, Catal. Lett. 127 (2009) 55–62.
[19] M. Piacentini, M. Maciejewski, A. Baiker, Appl. Catal. B 66 (2006) 126–136.
[20] M. Casapu, J.D. Grunwaldt, M. Maciejewski, F. Krumeich, A. Baiker, M. Wittrock, S. Eckhoff, Appl. Catal. B 78 (2008) 288–300.
[21] M. Casapu, J.-D. Grunwaldt, M. Maciejewski, M. Wittrock, U. Gobel, A. Baiker, Appl. Catal. B 63 (2006) 232–242.
[22] M. Casapu, J.D. Grunwaldt, M. Maciejewski, A. Baiker, M. Wittrock, U. Göbel, S. Eckhoff, Top. Catal. 42–43 (2007) 3–7.
[23] J.H. Kwak, D.H. Kim, J. Szanyi, C.H.F. Peden, Appl. Catal. B 84 (2008) 545–551.
[24] L. Lietti, P. Forzatti, I. Nova, E. Tronconi, J. Catal. 204 (2001) 175–191.
[25] H. Mahzoul, J.F. Brilhac, P. Gilot, Appl. Catal. B 20 (1999) 47–55.
[26] E. Fridell, H. Persson, B. Westerberg, L. Olsson, M. Skoglundh, Catal. Lett. 66 (2000) 71–74.
[27] R. Büchel, R. Strobel, F. Krumeich, A. Baiker, S.E. Pratsinis, J. Catal. 261 (2009) 201–207.
[28] N. Maeda, A. Urakawa, A. Baiker, J. Phys. Chem. C 113 (2009) 16724–16735.
[29] M. Adamowska, A. Krzton, M. Najbar, P. Da Costa, G.r. Djeĭga-Mariadassou, Catal. Today 137 (2008) 288–291.
[30] H. Abdulhamid, J. Dawody, E. Fridell, M. Skoglundh, J. Catal. 244 (2006) 169–182.
[31] E. Roedel, A. Urakawa, S. Kureti, A. Baiker, Phys. Chem. Chem. Phys. 10 (2008) 6190–6198.
[32] I. Nova, L. Castoldi, L. Lietti, E. Tronconi, P. Forzatti, F. Prinetto, G. Ghiotti, J. Catal. 222 (2004) 377–388.
[33] Y. Su, M.D. Amiridis, Catal. Today 96 (2004) 31–41.
[34] B. Westerberg, E. Fridell, J. Mol. Catal. A: Chem. 165 (2001) 249–263.
[35] A. Urakawa, N. Maeda, A. Baiker, Angew. Chem. Int. Ed. 47 (2008) 9256–9259.
[36] T. Szailer, J.H. Kwak, D.H. Kim, J.C. Hanson, C.H.F. Peden, J. Szanyi, J. Catal. 239 (2006) 51–64.
[37] M. Symalla, A. Drochner, H. Vogel, S. Philipp, U. Göbel, W. Müller, Top. Catal. 42–43 (2007) 199–202.
[38] H. Abdulhamid, E. Fridell, M. Skoglundh, Appl. Catal. B 62 (2006) 319–328.
[39] W.S. Epling, C.H.F. Peden, J. Szanyi, J. Phys. Chem. C 112 (2008) 10952–10959.
[40] D. James, E. Fourre, M. Ishii, M. Bowker, Appl. Catal. B 45 (2003) 147–159.
[41] F. Frola, M. Manzoli, F. Prinetto, G. Ghiotti, L. Castoldi, L. Lietti, J. Phys. Chem. C 112 (2008) 12869–12878.
[42] H.-K. Lin, C.-B. Wang, H.-C. Chiu, S.-H. Chien, Catal. Lett. 86 (2003) 63–68.
[43] C.M.L. Scholz, B.H.W. Maes, M. de Croon, J.C. Schouten, Appl. Catal. A 332 (2007) 1–7.
[44] Y. Ji, T.J. Toops, J.A. Pihl, M. Crocker, Appl. Catal. B 91 (2009) 329–338.
[45] W.S. Epling, G.C. Campbell, J.E. Parks, Catal. Lett. 90 (2003) 45–56.
[46] J.-S. Choi, W.P. Partridge, W.S. Epling, N.W. Currier, T.M. Yonushonis, Catal. Today 114 (2006) 102–111.